Sensitivity of the Simulated Tropical Intraseasonal Oscillation to Cumulus Parameterizations*

JIA Xiaolong[1,2†](贾小龙) and LI Chongyin[2,3](李崇银)

1 *National Climate Center, Beijing* 100081

2 *LASG, Institute of Atmospheric Physics, Chinese Academy of Sciences, Beijing* 100029

3 *Institute of Meteorology, PLA University of Science and Technology, Nanjing* 211101

(Received May 6, 2008)

ABSTRACT

The sensitivity of the simulated tropical intraseasonal oscillation or MJO (Madden and Julian oscillation) to different cumulus parameterizations is studied by using an atmospheric general circulation model (GCM)—SAMIL (Spectral Atmospheric Model of IAP LASG). Results show that performance of the model in simulating the MJO alters widely when using two different cumulus parameterization schemes—the moist convective adjustment scheme (MCA) and the Zhang-McFarlane (ZM) scheme. MJO simulated by the MCA scheme was found to be more realistic than that simulated by the ZM scheme. MJO produced by the ZM scheme is too weak and shows little propagation characteristics. Weak moisture convergence at low levels simulated by the ZM scheme is not enough to maintain the structure and the eastward propagation of the oscillation. These two cumulus schemes produced different vertical structures of the heating profile. The heating profile produced by the ZM scheme is nearly uniform with height and the heating is too weak compared to that produced by the MCA, which maybe contributes greatly to the failure of simulating a reasonable MJO. Comparing the simulated MJO by these two schemes indicate that the MJO simulated by the GCM is highly sensitive to cumulus parameterizations implanted in. The diabatic heating profile plays an important role in the performance of the GCM. Three sensitivity experiments with different heating profiles are designed in which modified heating profiles peak respectively in the upper troposphere (UH), middle troposphere (MH), and lower troposphere (LH). Both the LH run and the MH run produce eastward propagating signals on the intraseasonal timescale, while it is interesting that the intraseasonal timescale signals produced by the UH run propagate westward. It indicates that a realistic intraseasonal oscillation is more prone to be excited when the maximum heating concentrates in the middle-low levels, especially in the middle levels, while westward propagating disturbances are more prone to be produced when the maximum heating appears very high.

Key words: tropical intraseasonal oscillation, cumulus parameterization, diabatic heating profile

1. Introduction

The tropical intraseasonal oscillation is a dominant mode of variability in the tropical troposphere. Since detected by Madden and Julian (1971, 1972), many studies have been done to reveal its observed characteristics. In short, the MJO is characterized by the planetary scale with wave number one, and tends to propagate eastward with a period of approximately 30–70 days. In the vertical, the oscillation shows a baroclinic structure characterized by zonal wind anomalies in the lower troposphere, being out of phase with those in the upper troposphere. This oscillation also has an evident seasonality with larger amplitude during boreal winter-spring than summer (Li, 1991; Madden and Julian, 1994; Hendon and Salby, 1994). In the horizontal, the MJO convection over the Indian and the western Pacific Oceans is strongly coupled with the circulation as a mixed Kelvin-Rossby wave and propagates slowly eastward (Rui and Wang, 1990; Chao and Lin, 1994). In regions away from the convective region of the western Pacific, the oscillation is characterized by a Kelvin wave with more rapid eastward propagation (Slingo et al., 1996; Matthews, 2000; Sperber, 2003). Observations indicate that low-level moisture convergence

*Supported by the National Natural Science Foundation of China under Grant Nos. 40575027 and 40675051, and the Project of Chinese Academy of Sciences (ZKCX-SW-226).

†Corresponding author: jiaxl@cma.gov.cn.

occurs to the east of the main MJO convection as a consequence of the boundary layer friction which plays an important role in retaining the eastward propagation of this oscillation (Sperber, 2003; Jones and Weare, 1996; Maloney and Hartmann, 1998).

At present, performances of the Atmospheric General Circulation Models (AGCMs) in simulating the MJO are not very good. In the Atmospheric Model Intercomparision Project (AMIP), examinations of the ability of 15 AGCMs to simulate the tropical intraseasonal oscillation indicated (Slingo and Coauthors, 1996) that although most models show evidence of an eastward propagating anomaly in the velocity potential field, no model has captured the main characteristics of the intraseasonal oscillation found in the analysis. The majority of models produce intraseasonal signals with unrealistically high phase speeds, too low periods (<30 days), and unrealistically low amplitudes. Most models also do not capture the seasonality of the signals. Cumulus parameterization applied in an AGCM was regarded as the most likely element to produce better MJO representations. A study by Park et al.(1990) showed that the University of California, Los Angeles (UCLA) model, which used the original Arakawa and Schubert (1974) convective scheme, did not produce the intraseasonal oscillation. However, the Goddard Laboratory for Atmospheric Science (GLAS) model, which used the same Arakawa-Schubert convective scheme but confined the penetrative convection to below 340 hPa, simulated 20–60-day oscillations, although the simulated oscillations were weaker than the observed. Based on the comparison of various cumulus parameterizations in different models, Slingo et al. (1996) suggested that convective schemes closed on buoyancy tend to produce better MJO signals than those closed on moisture convergence. Wang and Schlesinger (1999) studied the effect of three different convective parameterizations on the simulated MJO in a single AGCM and results showed that moist convective adjustment (MCA; Manabe et al., 1965) produced the strongest MJO, while the modified Arakawa and Schubert (AS) scheme (Arakawa and Schubert, 1974) produced the weakest. In addition, they suggested that, for all the three convective schemes, the simulated MJO depends sensitively on the relative humidity criterion (RHC) for convective development. Maloney and Hartmann (2001) analyzed the sensitivity of MJO in the NCAR CCM3 to convective parameterization and the results indicated that the McRAS (Sud and Walker, 1999) scheme gave a most successful performance in simulating realistic MJO among three different schemes—Zhang and McFarlane (1995), Hack (1994), and McRAS, but the MJO simulated by using this scheme is not improved by increasing the boundary layer RHC, contrary to the results of Wang and Schlesinger (1999). Rajendran (2002) also investigated the performances of MCA scheme and Hack scheme in simulating the MJO and results showed that MCA scheme is better than Hack scheme. It was also studied on the simulated MJO (Lee et al., 2003) by using three different convective scheme—simplified Arakawa and Schubert scheme (SAS; Numaguti et al., 1995), Kuo (1974) scheme, and the MCA scheme, and results showed that the MJO is the strongest produced by MCA scheme, while the weakest by the SAS scheme. Recently, Liu et al. (2005) indicated that the MJO in the National Center for Atmospheric Research (NCAR) Community Atmosphere Model version 2 (CAM2) was markedly improved by implementing the Tiedtke (1989) convective scheme in place of the Zhang and McFarlane scheme (1995). Xue et al. (1996) and Qu and Zhang (2004) also studied the MJO simulated by a GCM developed by the Institute of Atmospheric Physics (IAP), Chinese Academy of Sciences. Li and Yu (2001) compared the MJO represented by a coupled model and the atmospheric component model and indicated that the coupled model gives a better performance. Jia et al. (2004) also analyzed the MJO simulated by the SAMIL-R42L9. These studies have obtained many interesting results, but it is still not clear that what physical and dynamical factors result in the different performances of GCMs in simulating the MJO.

This study will examine the MJO simulated by an AGCM, then study the sensitivity of the simulated MJO to different cumulus parameterizations, and also study the impacts of the diabatic heating profiles on the MJO simulation by sensitivity experiments with

different heating profiles.

2. Descriptions of the AGCM, the convective schemes, and the observational data

The general circulation model used in this study is the atmospheric component model of the Flexible Global Ocean-Atmosphere-Land System model (FGOALS) developed at the Institute of Atmospheric Physics (IAP) Laboratory for Numerical Modeling for Atmospheric Sciences and Geophysical Fluid Dynamics (LASG) (Wu et al., 1996). It is called SAMIL (Spectral Atmospheric Model of IAP LASG). This is a global spectral model of R42 (128×108 Gaussian grid points, equivalent resolution of 2.8125° longitude×1.66° latitude) and 9 sigma levels with the top level at 17 hPa (R42L9). It employs a unique dynamic core that removes a reference atmosphere to reduce systematic errors due to truncation and topography (Wu et al., 1997). The parameterization package includes the Slingo et al. (1996) scheme for radiation, the Slingo (1980, 1987) scheme for cloud diagnosis, and the Hottslag and Boville (1993) scheme for the boundary layer. Further details on the formulation of SAMIL are available in Wu et al. (1996, 1997) and Wang et al. (2005).

Two cumulus schemes are used here. One is the moist convective adjustment (MCA; Manabe et al., 1965) scheme which is employed to prevent the large-scale atmosphere from becoming statically unstable. At each time step, the atmospheric column is checked for moist instability layer by layer, starting from the lowest model layer. If the lapse rate between the two adjacent layers exceeds the moist adiabat lapse rate, the vertical mixing of heat and moisture is invoked and condensation is allowed during mixing. Any remaining supersaturation is then removed by large-scale condensation. As a result, the temperature and moisture profiles are adjusted towards moist adiabats. Thus, clearly the nature and the vertical transport of heat and moisture depend on the local instability of a layer.

The other scheme is the Zhang and McFarlane (ZM) cumulus scheme which is a mass flux scheme inspired by the convective parameterization of Arakawa and Schubert (1974). An updraft ensemble of entraining convective plumes, all having the same mass flux at cloud base, relaxes the atmosphere toward a threshold value of convective available potential energy. In-cloud saturated downdrafts commence at the level of minimum moist static energy. Detrainment of ascending plumes also begins at the level of minimum moist static energy. Therefore, only ascending plumes that can penetrate through the conditionally unstable lower troposphere are present in the ensemble. A Hack scheme (1994) accompanies the ZM scheme for simulation of the shallow convection.

AMIP type runs are conducted for 12 yr from 1 January 1978 to 31 December 1989. The first year of integration was ignored. Daily mean outputs in winds, precipitation, divergence, humidity, vertical velocity, and diabatic heating are used for MJO diagnosis. The validation data were extracted from NCEP/NCAR reanalysis (Kalney et al., 1996) and the Climate Prediction Center (CPC) merged precipitation data (CMAP) (Xie and Arkin, 1996). In order to identify the intraseasonal variability, climatology for 11 yr was first subtracted from daily mean data, and then a 30–60-day band-pass filter was applied. Power spectra, empirical orthogonal function (EOF), and linear regression were applied to analyze modeled MJO features.

3. Comparison of MJO characteristics simulated by two cumulus schemes

3.1 Longitude-time sections

The basic diagnosis for identifying the intraseasonal oscillation is the time-longitude diagram. For brevity, Fig.1 only shows the time-longitude diagrams of the 30–60-day filtered 850-hPa zonal wind (U850) averaged between 10°S and 10°N from NCEP and that simulated by SAMIL-R42L9 for 1980. Seen from the NCEP analyses (Fig.1a), the MJO is characterized by eastward propagating disturbances with a typical period of 45 days, but also moves westward occasionally. In the horizontal, this oscillation shows the planetary scale of wave numbers 1–3, and its phase speed often appears to be faster over the Western Hemisphere with

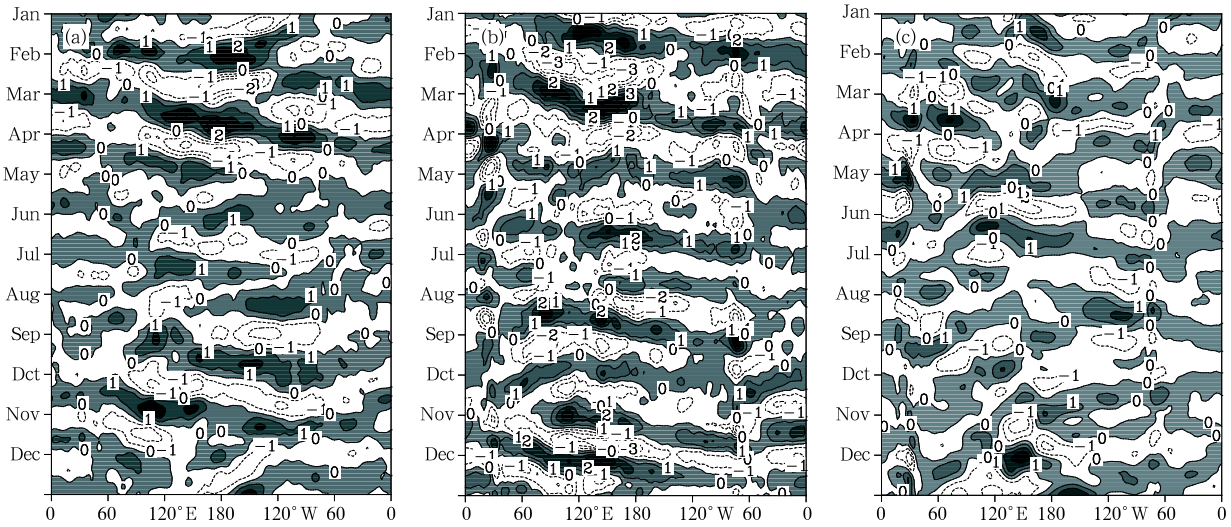

Fig.1. Time-longitude diagrams of the 30–60-day filtered 850-hPa zonal wind (m s^{-1}) averaged between 10°S and 10°N from NCEP (a) and that simulated by SAMIL-R42L9 with the MCA scheme (b) and the ZM scheme (c) for 1980. The contour interval is 1 m s^{-1}, and positive values are shaded.

15 m s^{-1} than that over the Eastern Hemisphere with 4–6 m s^{-1}. The MCA scheme also produced a number of eastward moving disturbances at the intraseaonal time scales with relative amplititudes comparable to the NCEP reanalysis and even larger in some years. Intraseasonal signals produced by the ZM scheme are very weak and show little eastward propagation.

3.2 Time-space spectral analysis

Characteristic scales and periods of propagating components in the intraseasonal variability shown in Fig.1 are further investigated by using time-space power spectra. The 11-yr climatology was first subtracted from daily mean 850-hPa zonal wind and precipitation to derive anomalous series to remove high and low frequency disturbances, and then time-space spectra were calculated by using the anomalies of 850-hPa zonal wind and precipitation, both averaged over 10°S–10°N for each year. In Fig.2, the vertical axis denotes zonal wave numbers, and the horizontal axis represents periods with positive (negative) values corresponding to eastward (westward) propagation. The NCEP 850-hPa wind spectrum is dominated by the power at wave number 1 and eastward propagation with periods of 30–70 days, with peaks occurring at approximately 45.6, 60, and 30 days, respectively (Fig.2a). The spectrum of precipitation (Fig.2b) shows a wider range of dominant zonal wave numbers. There are also much power spectra over wave numbers 2–4. Eastward propagation is also dominated by the period of 30–60 days with the maximum spectrum occurring at about 45 days. These results are consistent with the results of other studies although length and range of data used for time-space power spectra analysis are different. Seen from Fig.2c, the MCA scheme produces a strong eastward propagating power spectrum of U850 at the intraseasonal time scale and strong power spectra is also mainly on wave number one with typical periods at 73, 45.6, and 36 days, meanwhile, the spectrum of westward propagation is much weaker than that of eastward propagation. Precipitation shows similar power spectra to U850 though it has more dispersed power spectra at the time and spatial scale as shown in Fig.2d. The U850 produced by the ZM scheme shows little power spectra at the intraseasonal time scale and the power spectra for eastward propagating wave is close to that for westward propagating wave with the maximum power at wave number 4 (Fig.2e). Just as shown in Fig.1, the MJO produced by the ZM scheme is very weak and shows little propagation.

3.3 Propagating characteristics

In order to better demonstrate the propagation

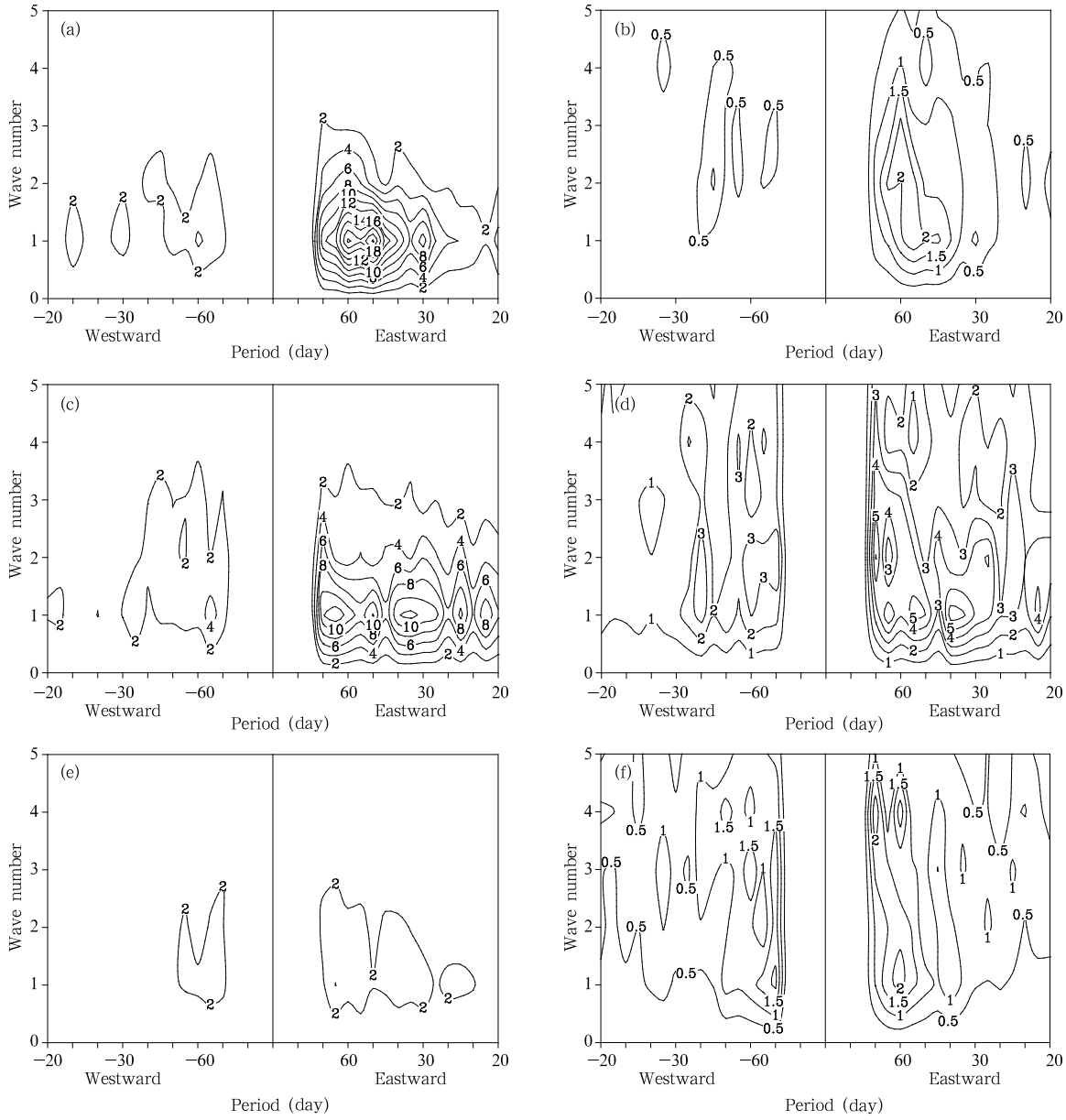

Fig.2. Space-time power spectra of 850 hPa zonal wind (m^2 s^{-2}) and precipitation (mm^2 day^{-2}) averaged between 10°S and 10°N. (a) U850 from NCEP, (b) precipitation from Xie/Arkin, (c) U850 from MCA, (d) precipitation from MCA, (e) U850 from ZM, and (f) precipitation from ZM.

characteristics and amplitude of intrasesonal U850 along the equator, a lagged linear regression was used here. Based on observations, the maximum MJO amplitude is located over the western Pacific and the Indian Ocean (Salby and Hendon, 1994), therefore, following Maloney and Hartmann (2001), we select 150°E as a reference point. U850 data were filtered by 30–60 days, and averaged over 10°S to 10°N at every equatorial longitude, and then regressed onto the zonal wind time series at 150°E. All regressions have been scaled by 1-std-dev (standard deviation) perturbation of zonal wind time series at 150°E. Figure 3a shows the lag-regression plots for U850 from the NCEP reanalysis. It can be seen that the intraseasonal 850-hPa wind propagates coherently from the Indian to Pacific Oceans with periods of approximately 45 days, and

its phase speed appears to be faster over the Western Hemisphere than that over the Eastern Hemisphere with a discontinuity near the dateline. These results are consistent with those of other observational studies (Maloney and Hartmann, 2001; Sperber, 2003). The MCA scheme reproduces the eastward propagated intraseasonal 850-hPa wind with periods of about 40 days and the similar amplitude to NCEP reanalysis. And it also simulated the changes of propagating speed between the Western Hemisphere and the Eastern Hemisphere (Fig.3b). Signals produced by the ZM scheme show little propagated signals and its amplitude is also very weak (Fig.3c).

4. Life cycle of composite Madden-Julian oscillation

4.1 MJO index

Following Maloney and Hartmann (1998), an MJO index was devised in order to further analyze the structure of simulated MJO. U850 data filtered by 30–60 days from 1 Jan 1979 to 31 December 1989 were averaged between 10°S and 10°N, and then an empirical orthogonal function (EOF) analysis was applied to the zonal wind time series. Figure 4a shows the first two EOFs from NCEP reanalysis explaining 37.4% and 26.2% of the total bandpass-filtered variance, respectively. The first two EOFs are analogous spatially. The lag correlation between PC1 and PC2 indicates that their lag correlation coefficients arrive the maximum (above 0.7) when PC2 lags behind PC1 by 11 days (Fig.4b). Thus, an eastward propagating signal is described by EOF1 and EOF2 in the equatorial U850. Figure 4c are EOFs simulated by the MCA scheme, and the PC2 is correlated with PC1 at 0.6 when PC2 lags behind PC1 by 9 days (Fig.4d), which indicates an eastward propagation from EOF1 to EOF2. Because EOF1 and EOF 2 in the ZM scheme

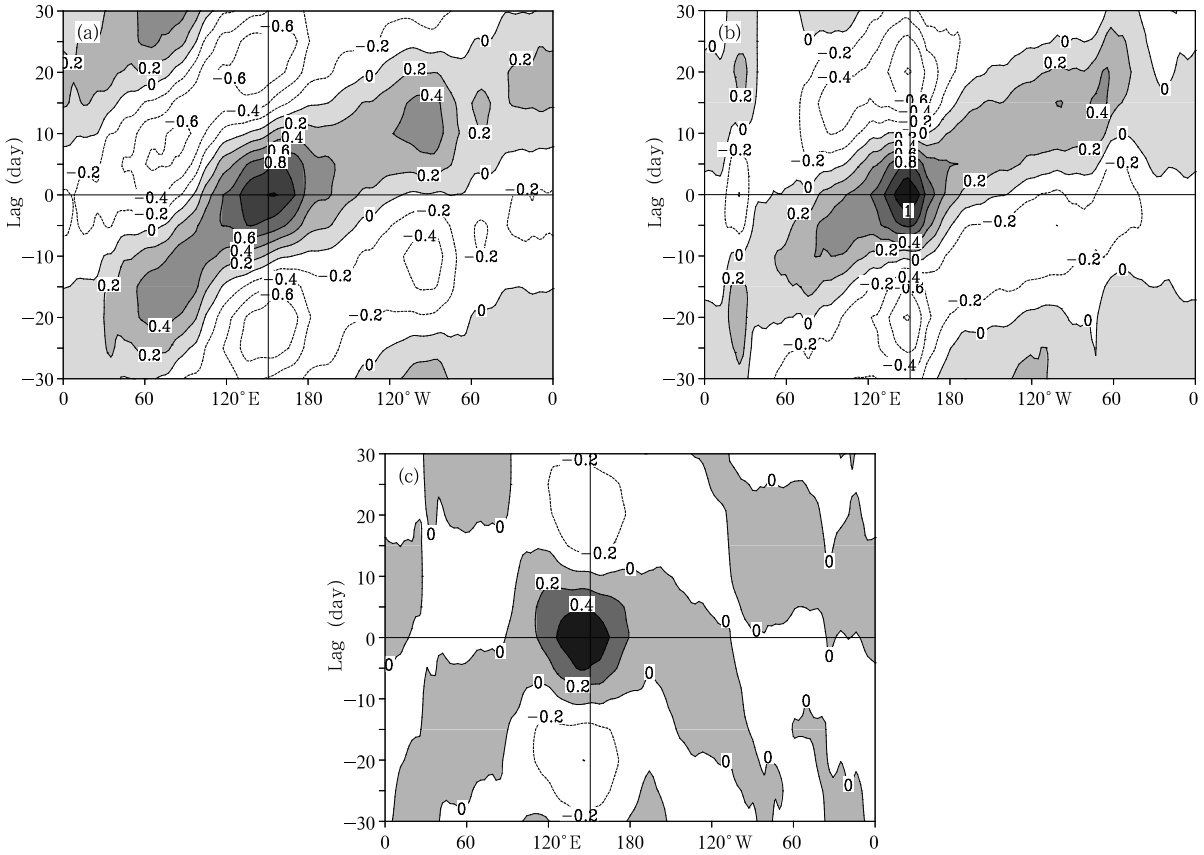

Fig.3. Lag regression plot of 850-hPa zonal wind averaged over 10°S–10°N as a function of longitude from NCEP (a), and simulations with the MCA scheme (b) and ZM scheme (c). The reference time series is at 150°E.

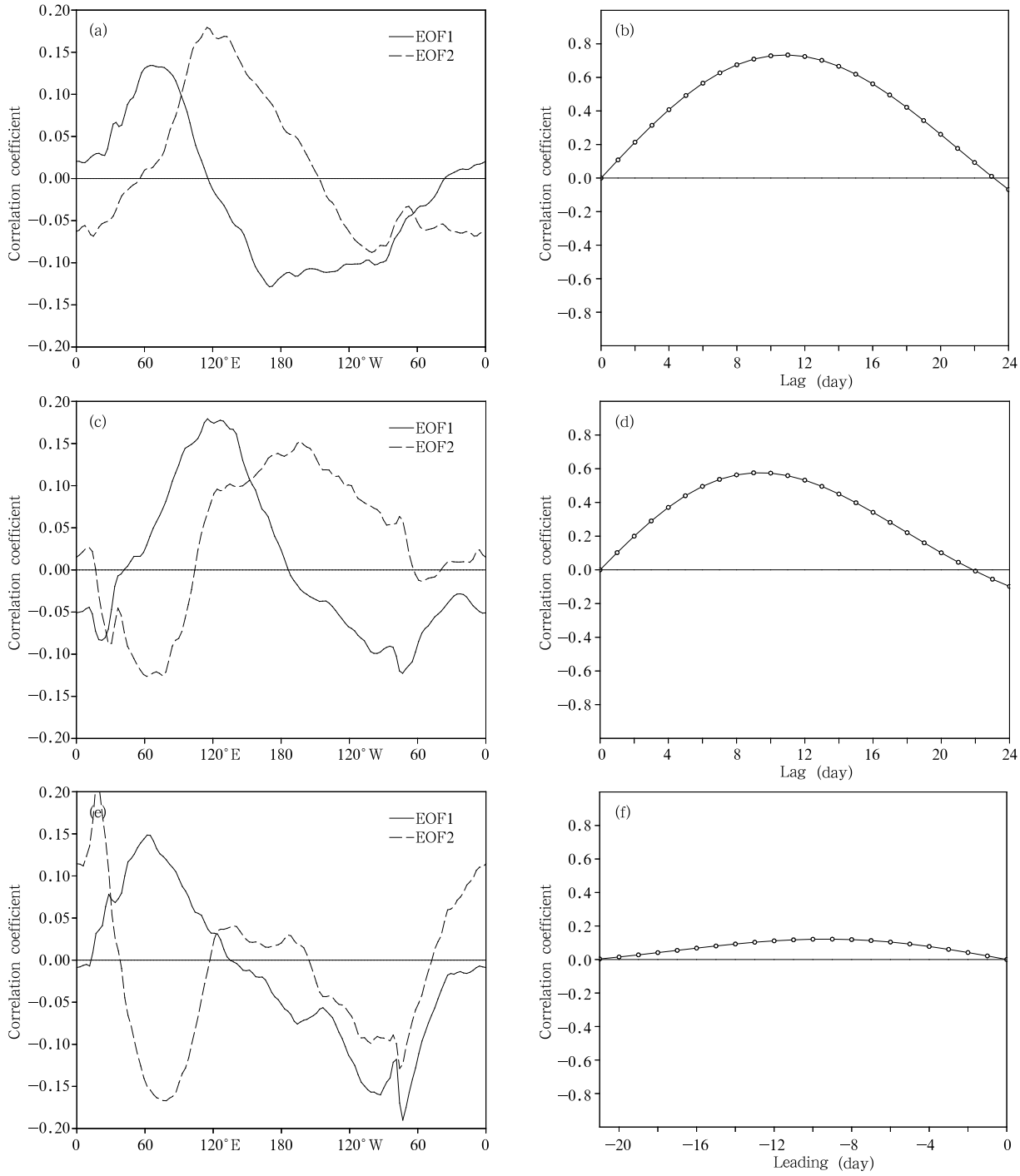

Fig.4. First two EOFs of the 10°S–10°N averaged 30–60-day bandpass filtered U850 from the NCEP (a), and simulations with MCA scheme (c) and ZM scheme (e). Time lag correlations between corresponding PC1 and PC2 for NCEP (b), MCA scheme (d) and ZM scheme (f) are also shown.

do not show analogous shape and no significant correlation exits between the PC1 and PC2 (less than 0.15), then no clear propagation can be suggested (Figs.4e and 4f).

Because the lagging correlation between the PC1 and PC2 similar to the reanalysis are well captured by

the MCA scheme, then following Maloney and Hartmann (1998), two MJO indexes as a linear combination of the PC1 and PC2 based on the lag-correlation equal to or greater than 0.4, can be defined for the NCEP reanalysis and the MCA scheme, as follows:

$$\text{NCEP}: \text{index}_1(t) = \text{PC1}(t) + [\text{PC2}(t+4) + \cdots + \text{PC2}(t+18)]/15.$$

$$\text{MCA}: \text{index}_2(t) = \text{PC1}(t) + [\text{PC2}(t+5) + \cdots + \text{PC2}(t+15)]/11.$$

where t is the time in day.

4.2 Life cycle of the simulated MJO

In order to explore the space-time structure of the MJO, the MJO index time series is linearly regressed against numerous variables. Linear regressions of the MJO index for NCEP with 30–60-day band filtered U850, precipitation and 850-hPa specific humidity from time lags of –20 to 20 days are shown in Fig.5 , and same regressions but with 1000-hPa and 850-hPa divergences are shown in Fig.6. It is clear that the MJO convection first appears over the western Indian Ocean at day –20 accompanied by anomalous easterlies and positive specific humidity anomalies (Fig.5). Anomalous convergence at 1000-hPa leads that at 850-hPa, and occurs to the east of the main MJO convection (Fig, 6). By day –10, precipitation strengthens and propagates eastward over the Indian Ocean, in conjunction with the eastward propagating 850-hPa wind and low-level positive moisture anomalies (Fig.5). The 850-hPa anomalous convergence also strengthens and extends eastward over the whole Indian Ocean, while the 1000-hPa convergence further extends into the Maritime Continent and the West Pacific (Fig.6). By day 0, the 850-hPa wind anomalies match the first EOF mode shown in Fig.4. The maximum westerly anomaly is over the Indian Ocean, and the mid-eastern Pacific is dominated by easterly anomalies, and the anomalous precipitation also propagates eastward into the western Pacific accompanied by 850-hPa anomalous convergence. The 1000-hPa anomalous convergence and the positive moisture anomalies are nearly in phase and lead the 850-hPa anomalous convergence. By day 10, the 850-hPa wind anomalies match the second EOF mode shown in Fig.4. The maximum westerly anomalies propagate eastward into the Maritime Continent and the West Pacific, and the main convection is also located over the western Pacific, while the negative precipitation anomaly is located over the Indian Ocean (Fig.5). The 850-hPa anomalous convergence is in phase with the anomalous precipitation, while the 1000-hPa anomalous convergence is located over the eastern Pacific and southern America (Fig.6). By day 20, the positive precipitation anomalies propagate into the southern Pacific and the South China Sea, and the maximum westerly anomalies are located over the central Pacific. By day 30 (figure omitted), the MJO precipitation appears again over the western Indian Ocean accompanied by low-level easterlies anomalies and positive moisture anomalies and anomalous convergence at 1000 hPa, which indicates the beginning of a new MJO life cycle.

During the life cycle of the MJO, a mixed Kelvin-Rossby wave structure is manifested in 850-hPa winds with a resembled Kelvin wave structure at near-equator and a Rossby wave structure in tropics away from the equator. Furthermore, the 1000-hPa anomalous convergence always leads the 850-Pa anomalous convergence and the MJO convection anomalies, which has been considered to play an important role in maintaining MJO eastward propagation. These results are consistent with other observational analysis (Madden and Julian, 1994; Jones and Weare, 1996; Maloney and Hartmann, 1998; Sperber, 2003).

The evolvement of variables associated with the MJO can be further illustrated using longitude time lag plots of the linear regression of MJO index with the averaged (10°S–10°N) band-pass filtered 850-hPa zonal wind, precipitation, 500-hPa vertical velocity, 850-hPa specific humidity, 1000- and 850-hPa divergence, as shown in Fig.7. All variables are dominated by eastward propagating signals, especially over the Eastern Hemisphere. The initial MJO rainfall and U850 appear over the western Indian Ocean and then propagate eastward with amplified amplitudes and then weaken and disappear across the dateline, and the wind signals continue to propagate eastward

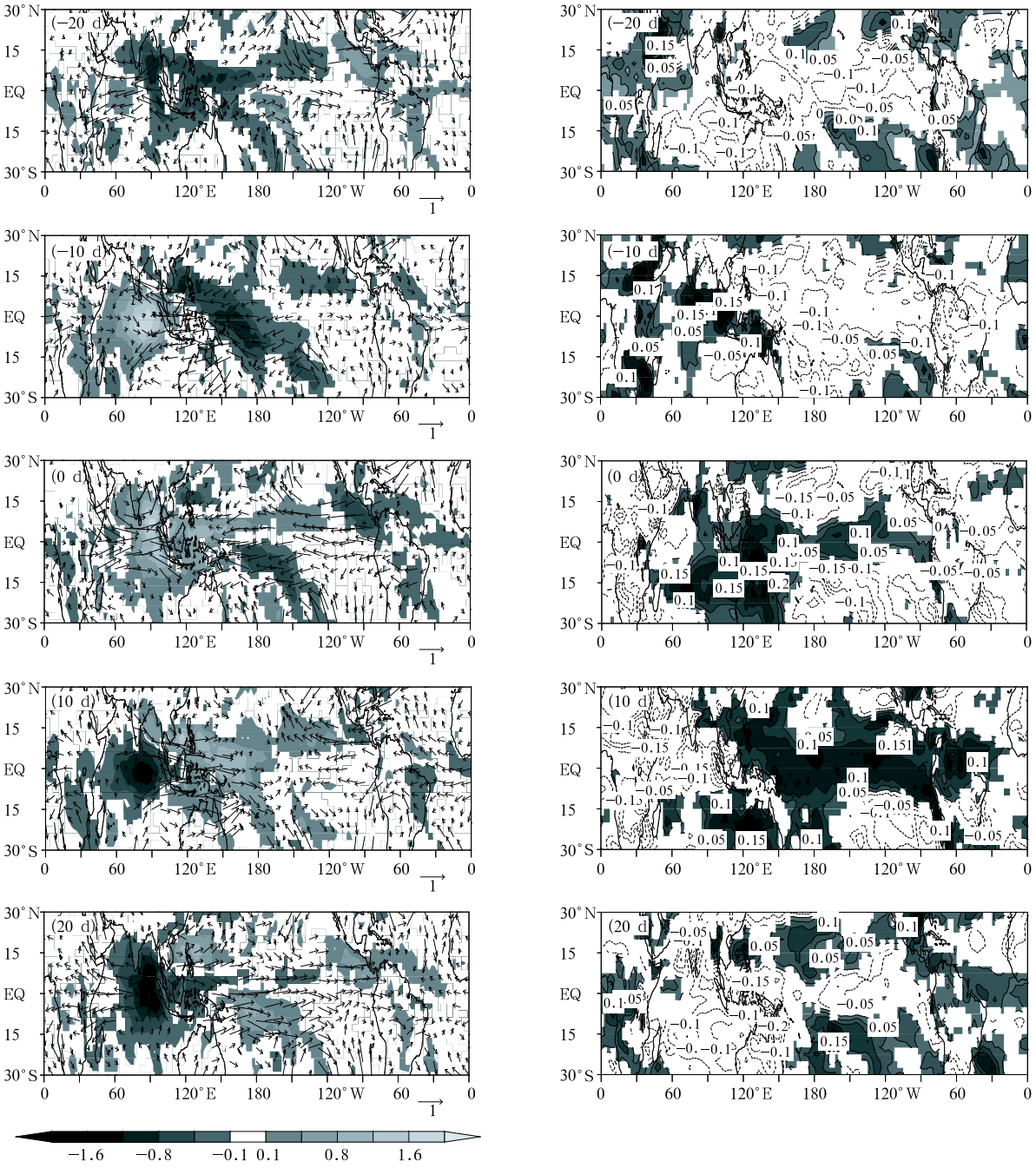

Fig.5. Linear regressions of MJO index for NCEP with 30–60-day bandpass-filtered 850-hPa wind (m s^{-1}) and rainfall (mm day^{-1}) from time lags –20 to 20 days (left panels). The right panels show linear regressions of MJO index with 850-hPa specific humidity (g kg^{-1}). Positive values are shaded.

with more rapid speeds. The 500-hPa vertical motion, 850-hPa divergence, and 850-hPa moisture anomalies are all closely in phase with rainfall anomalies, while the 1000-hPa divergence leads to rainfall anomalies (Fig.7).

Figures 8 and 9 show results from the MCA scheme. The MJO precipitation first appears over the Africa and western Indian Ocean on day –10 accompanied by anomalous easterlies and positive specific humidity anomalies (Fig.8) and the anomalous conver-

gence at 1000 and 850 hPa (Fig.9). By day 0, precipitation strengthens further and propagates eastward over the whole Indian Ocean, in conjunction with low level positive moisture anomalies (Fig.8), the 1000- and 850-hPa anomalous convergence, and the 1000-hPa convergence slightly leads the 850-hPa convergence (Fig.9). By day 10, rainfall anomalies extend eastward into the Maritime Continent, and the western Pacific Ocean is dominated by 850-hPa easterly anomalies, positive moisture anomalies and anomalous convergence. By day 20, the 850-hPa wind and rainfall anomalies continue propagating eastward into the mid-eastern Pacific, and accompanied by low-level positive moisture anomalies.

Figure 10 further displays longitude-lag plots of MJO variables from the MCA scheme. The 850-hPa wind anomalies propagate eastward coherently with higher speed over the Western Hemisphere than over the Eastern Hemisphere. Eastward propagating rainfall anomalies are mainly located over the convergent

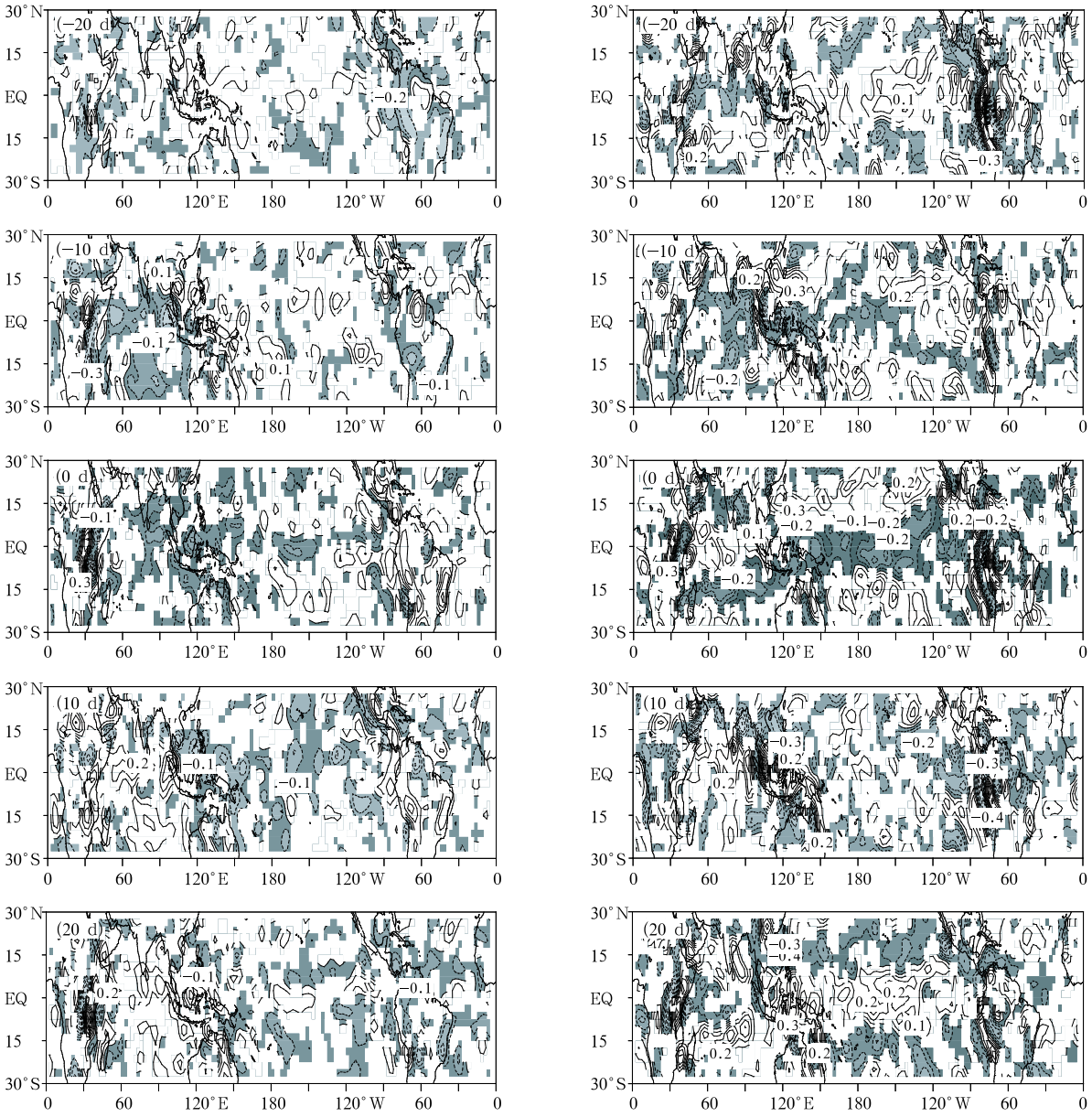

Fig.6. As in Fig.5, but for 30–60-day band-pass filtered 850-hPa (left panels) and 1000-hPa (right panels) divergence. Negative values are shaded, unit: $10^6 s^{-1}$.

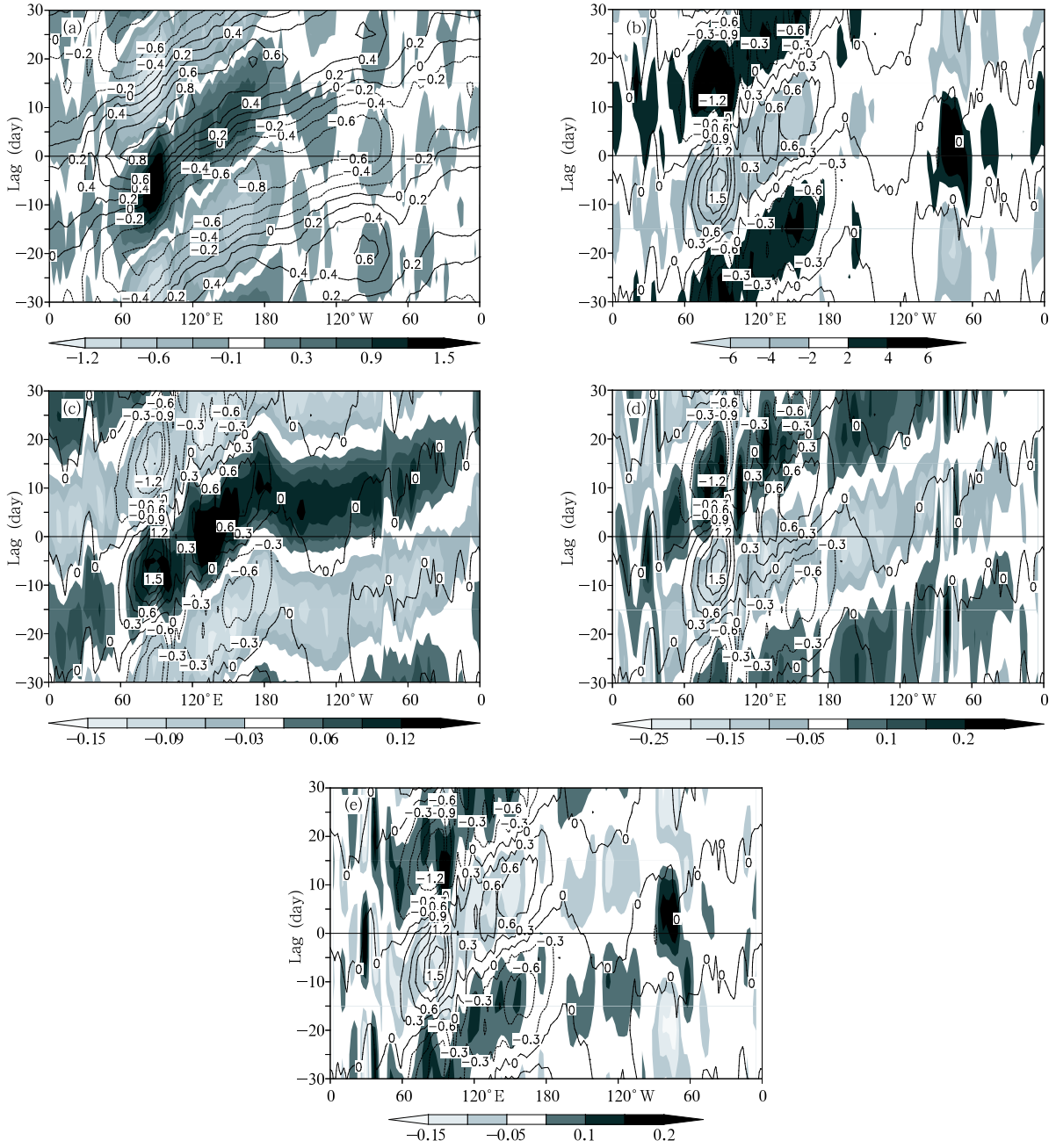

Fig.7. Longitude-time lag plots of the linear regression of MJO index for NCEP with 10°S–10°N averaged 30–60-day band-pass filtered for (a) U850 (contours, m s^{-1}) and rainfall (shaded, mm day^{-1}), (b) rainfall (contours, mm day^{-1}) and 500-hPa vertical velocity (shaded,10^{-3} hPa s^{-1}), (c) rainfall (contours, mm day^{-1}) and 850-hPa specific humidity (shaded, g kg^{-1}), (d) rainfall (contours, mm day^{-1})and 1000 hPa divergence (shaded, 10^6 s^{-1}), and (e) rainfall (contours, mm day^{-1}) and 850-hPa divergence (shaded, 10^6 s^{-1}).

zone of westerly and easterly anomalies and slightly to the easterly zone. In addition, there are too many MJO precipitation signals propagating into the eastern Pacific Ocean compared to the reanalysis (Fig.10a). Eastward propagating rainfall signals are accompanied by upward motion (Fig.10b) and low-level positive

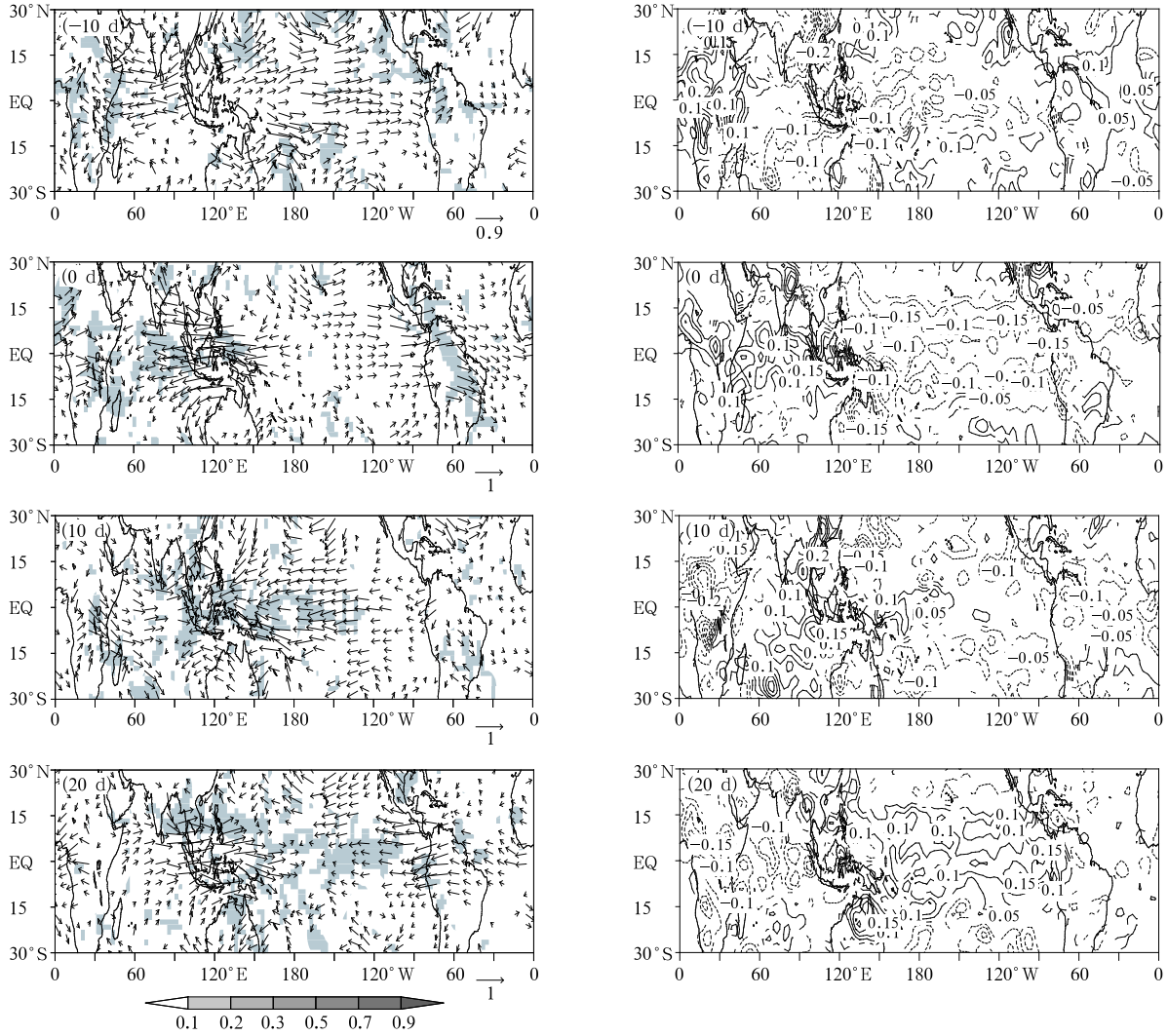

Fig.8. Linear regressions of MJO index for MCA scheme with 30–60-day band pass-filtered 850 hPa wind (m s^{-1}) and rainfall (shaded, mm day^{-1}) from time lags –10 to 20 days (left panels). The right panels show linear regressions of MJO index with 850 hPa specific humidity (g kg^{-1}). Positive values are shaded.

moisture anomalies (Fig.10c). The 1000-hPa convergence slightly leads rainfall (Fig.10d), and the 850-hPa convergence is in phase with rainfall signals (Fig.10e).

For the ZM scheme, because the first two PCs of the 850-hPa wind do not show any lag correlation as shown in Fig.4, the regressed MJO fields either by PC1 or PC2, including 850-hPa winds, precipitation, divergence and moisture, show little organized propagation (figure omitted). Figure 11 displays longitude-time lag plots of MJO variables from the ZM scheme. It can be seen that no eastward propagating signals can be found in both 850-hPa wind and precipitation (Fig.11a). Low-level moisture and upward motion are very weak over the Indian Ocean and the western Pacific (Figs.11b, c), and there is no strong low-level convergence in the process of MJO evolvement, which does not favor the cumulus convective heating and the maintaining and propagating of the MJO.

5. Vertical heating profile

Li (1983) suggested that the maximum heating over the mid-low troposphere can excite an unstable mode similar to the observed tropical 30–60-day

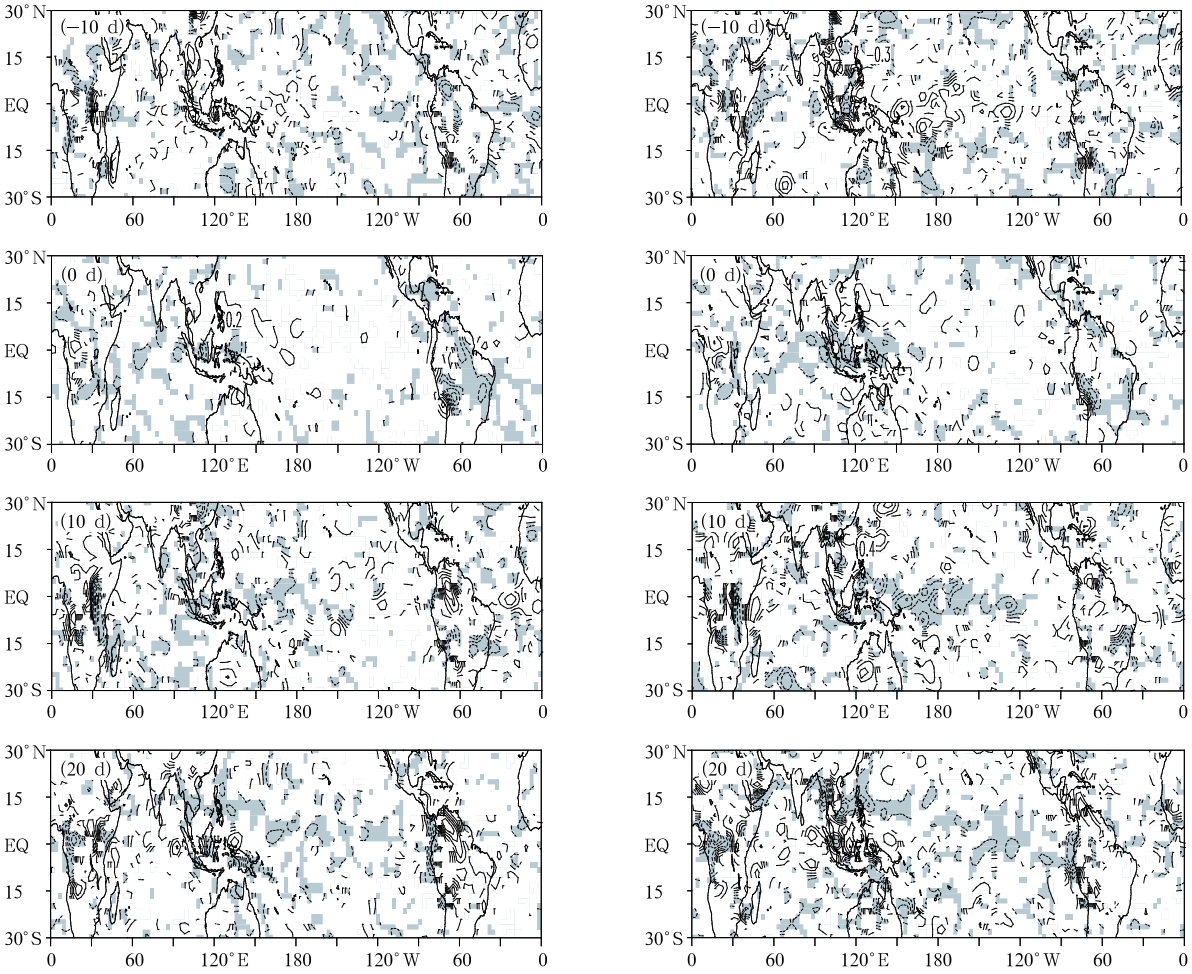

Fig.9. As in Fig.8, but for 30–60-day band-pass filtered 850-hPa (left panels) and 1000-hPa (right panels) divergence. Negative values are shaded, unit: 10^6 s^{-1}.

oscillation. Simple theoretic studies by Lau and Peng (1987) and Sui and Lau (1989) also indicate that the phase speed of MJO is sensitively dependent on the vertical structure of the convective heating, the height of maximum heating being higher, the phase speed of the oscillation being faster. The heating profile produced by the UCLA model using the Arakawa and Schubert (1974) convective scheme shows a nearly uniform heating rate with height through the troposphere. Similarly, the UCLA model also gives a weak simulated MJO (Park et al., 1990).

Figure 12 displays the mean diabatic heating profiles produced by the two schemes over the western Pacific (10°N–10°S, 120°E–180°) during the phase of MJO with maximum precipitation. The heating profile produced by the MCA scheme has an evident maximum concentrated in the mid-troposphere, and the maximum heating shows a clear extension downward. According to the theory of Sui and Lau (1989), this downward extension of the maximum heating must be reflected in the phase speed of MJO, leading to slower speed in the MCA scheme with the most prominment period of 73 days as shown in Fig.2. Compared with the MCA scheme, the heating produced by the ZM scheme is very weak, with the maximum heating of 1.0 and 1.5°C day^{-1} for winter and summer respectively. Another noticeable feature is the heating profile produced by the ZM scheme shows a nearly uniform heating rate with height through the troposphere, and the height of the maximum heating is much higher than that by the MCA scheme.

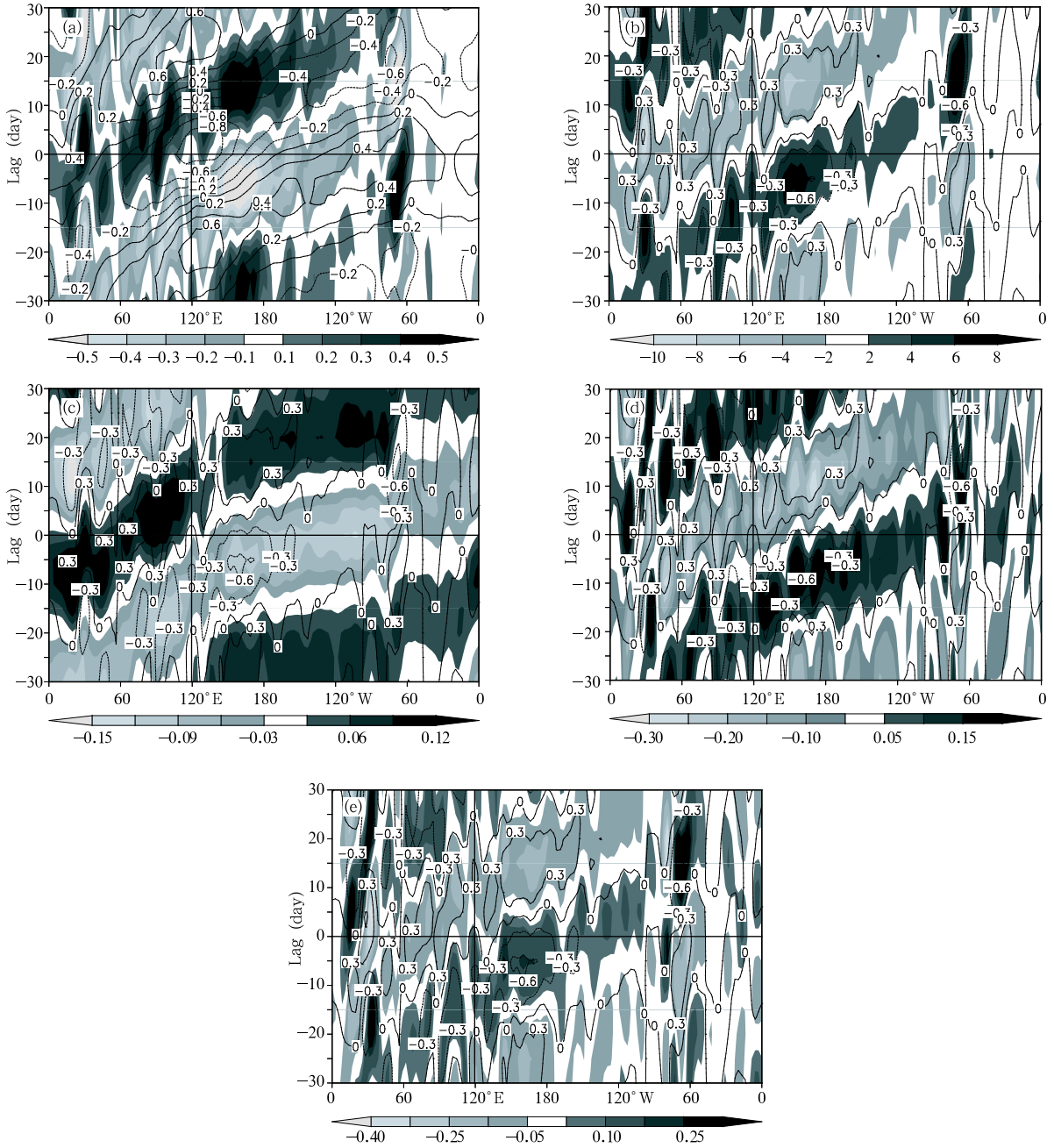

Fig.10. As in Fig.7, but for the MCA scheme.

6. Sensitivity experiments with different vertical heating profiles

In order to investigate the sensitivity of simulated MJO to different vertical heating structures, here three simple experiments are conducted by changing the vertical structure of the diabatic heating produced by the model. This was done via multiplying the model generated (parameterized) convective heating by a given set of coefficients shown in Fig.13 in the tropics (20°S–20°N) before they were passed to the temperature tendency equation. Three simulations were thus made, with their modified heating profiles respectively peaking in the upper troposphere (i.e., "upper-level heating", hereafter referred to as UH), middle troposphere (MH), and lower troposphere

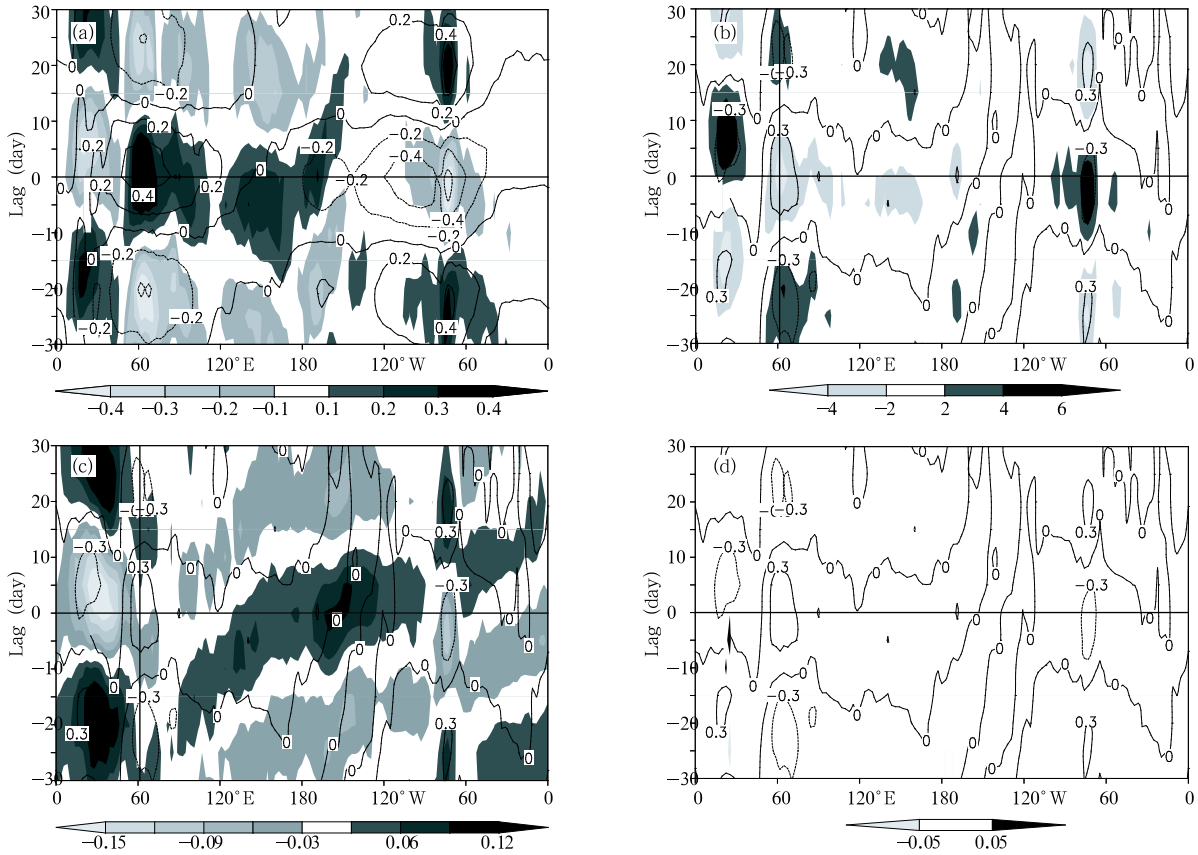

Fig.11. Longitude-time lag plots of the linear regression of PC1 for the ZM scheme with 10°S–10°N averaged 30–60-day band-pass filtered (a) U850 (contours, m s^{-1}) and rainfall (shaded, mm day^{-1}), (b) rainfall (contours, mm day^{-1}) and 500-hPa vertical velocity (shaded, 10^{-3} hPa s^{-1}), (c) rainfall (contours, mm day^{-1}) and 1000-hPa specific humidity (shaded, g kg^{-1}), and (d) rainfall (contours, mm day^{-1}) and 1000-hPa divergence (shaded, 10^{6} s^{-1}).

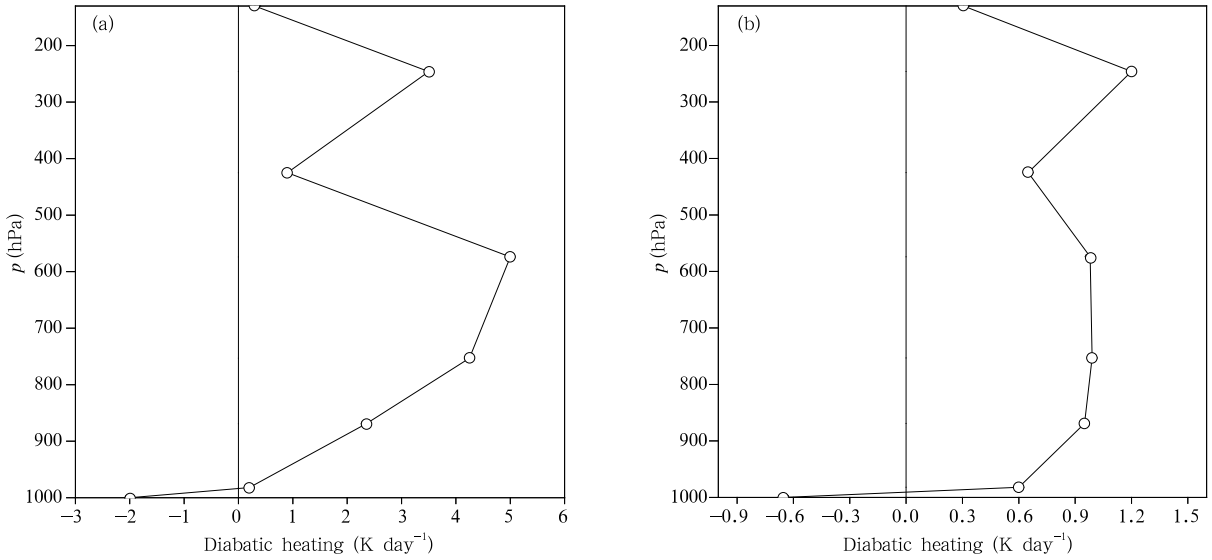

Fig.12. Vertical profiles of diabatic heating in the western tropical Pacific produced by the MCA scheme (a) and the ZM scheme (b), based on the maximum 30–60-day band-pass filtered rainfall in the region 10°S–10°N, 120°E–180°.

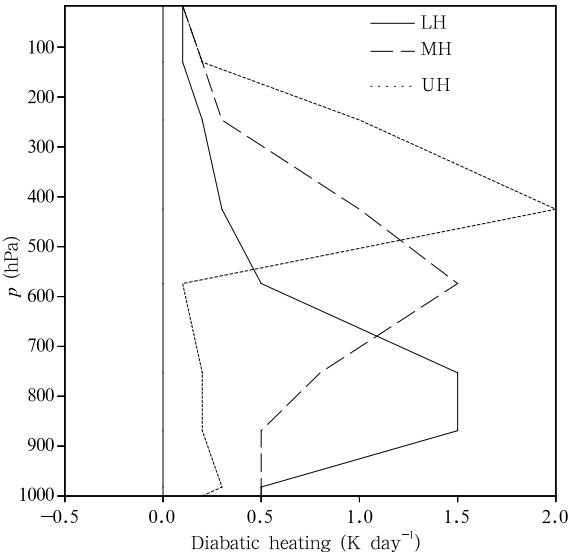

Fig.13. Coefficients multiplied in HH, MH, and LH experiments.

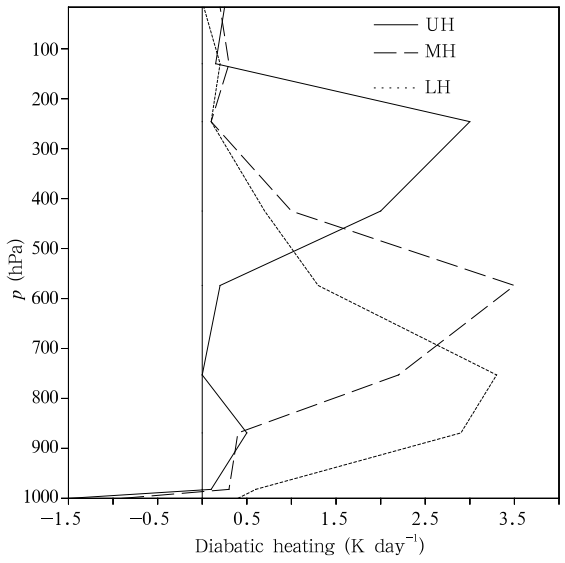

Fig.14. Vertical profiles of diabatic heating in the western tropical Pacific simulated in HH, MH, and LH experiments (K day^{-1}).

(LH), as shown in Fig. 14. Three simulations were all forced by the climatological monthly SSTs and were integrated for 3 yr.

Figure 15 displays the time lag correlation coefficients with 30–60-day band-pass filtered 850-hPa zonal wind averaged over 10°S–10°N based on the reference point of 150°E as in Fig.3. The intraseasonal U850 produced by the UH experiment propagates westward, while those by MH and LH propagate eastward. Figure 16 shows the space-time spectra of 10°S–10°N averaged 850-hPa zonal wind produced by three experiments. It can be seen that the intraseasonal westward moving power is obviously much stronger than the eastward moving power in the UH run, which indicates that when the maximum heating rate is located at the high level of the troposphere, the model more likely produces westward propagating disturbances on the intraseasonal time scales. In the MH and LH runs, the intraseasonal eastward moving power is much stronger than the westward moving power. Through the comparison with the spectrum from the NCEP reanalysis, the westward moving power in both MH and LH runs is too large, especially in the LH. It also indicates that the maximum heating at the middle or low levels of the troposphere is more favorable to produce the intraseasonal signals similar to observations.

7. Conclusions and discussion

The sensitivity of the simulated MJO to different cumulus parameterizations is studied by the atmospheric general circulation model—SAMIL. In the present paper, results from two cumulus parameterization schemes are compared, the moist convective adjustment (MCA) and the Zhang-McFarlane (ZM) scheme. Main conclusions can be drawn as follows:

(1) The performance of the SAMIL model in simulating the MJO is highly sensitive to cumulus parameterizations implanted in. The MJO simulated by the MCA scheme was found to be more realistic than that by the ZM scheme, at aspects of the phase speed, period, power spectra, the intraseasonal timescales, eastward propagation, and life cycle.

(2) The MJO produced by the ZM scheme is too weak and shows little propagation characteristics. Weak moisture convergence at low levels simulated by the ZM scheme is inadequate to maintain the structure and the eastward propagation of the oscillation.

(3) These two cumulus schemes have produced heating profiles with different vertical structures. The heating profile in the ZM scheme is nearly uniform with height and the heating strength is too weak compared to that produced by the MCA scheme. This

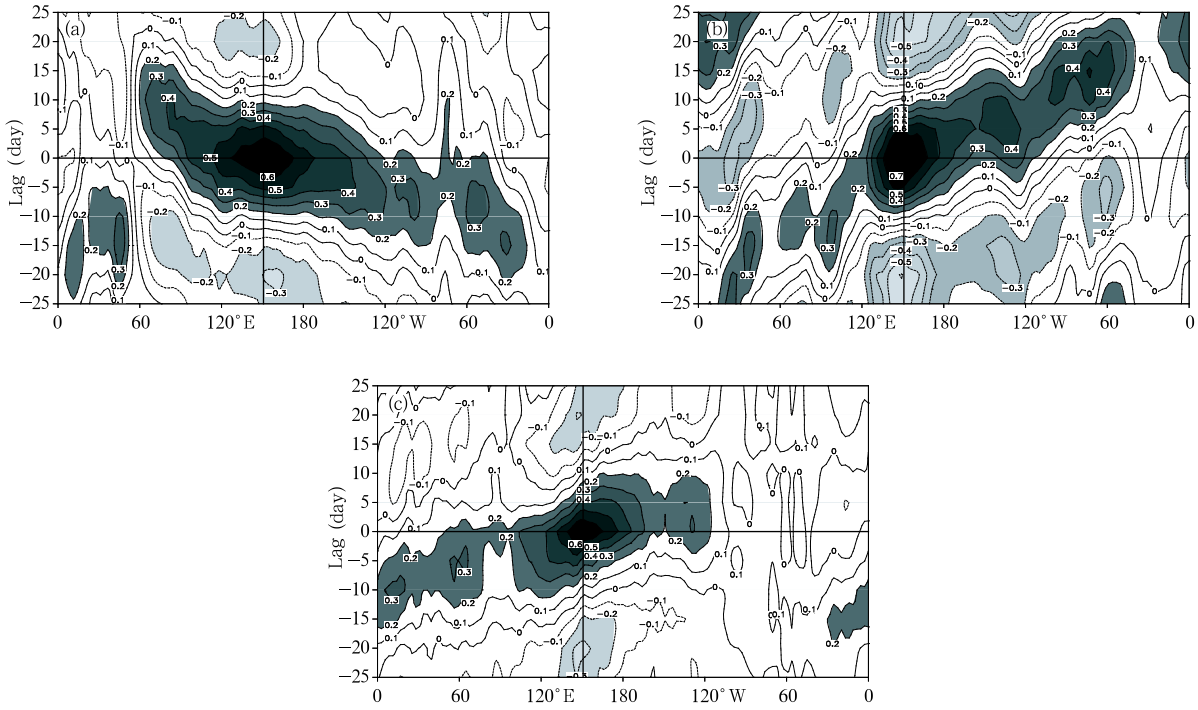

Fig.15. Time lag correlation coefficients of 30–60-day band-pass filtered 850-hPa zonal wind averaged over 10°S–10°N as a function of longitude from experiments UH (a), MH (b), and LH (c). The reference time series is at 150°E.

maybe contributes greatly to the failure of simulating a reasonable MJO. For different cumulus parameterization schemes, the diabatic heating profiles produced by them play an important role in the performance of the GCM.

(4) Three sensitivity experiments with different heating profiles are designed in which modified heating profiles peak respectively in the upper troposphere (UH), middle troposphere (MH), and lower troposphere (LH). Both the LH and MH runs produce eastward propagating signals at the intraseasonal timescale, while it is interesting that the intraseasonal timescale signals produced by the UH run propagate westward. It indicates that realistic intraseasonal oscillation is more prone to be excited when the maximum heating concentrating in the middle-low level, especially in middle levels, while westward propagating disturbances at the intraseasonal time scale are more prone to be produced when the height of the maximum heating is very high.

It is interesting that the MCA scheme always gives a relatively good MJO simulation than other convective schemes in many other AGCMs. For example, the Goddard Laboratory for Atmospheric Science (GLAS) model using the MCA scheme gives better MJO eastward propagating than using the Recharged Arakawa and Schubert (1974) scheme and the simple convective scheme by Chao and Lin (1994) (Chao and Deng, 1998). The University of Illinois, Urbana–Champaign (UIUC) atmospheric general circulation model also gives a better MJO simulation when using the MCA scheme than using the modified Arakawa-Schubert penetrative-convection parameterization (1974) and the parameterization of Kuo (1974). The MCA scheme also gives a better MJO simulation in the National Center for Atmospheric Research (NCAR) Community Climate Model Version 2.0 (CCM2) than the Hack scheme (1994) (Rajendran et al., 2002). The ZM scheme used here is also used in the standard CCM3 and CAM2 (Community Atmosphere Model Version 2.0), and studies found these two models produced an MJO signal with

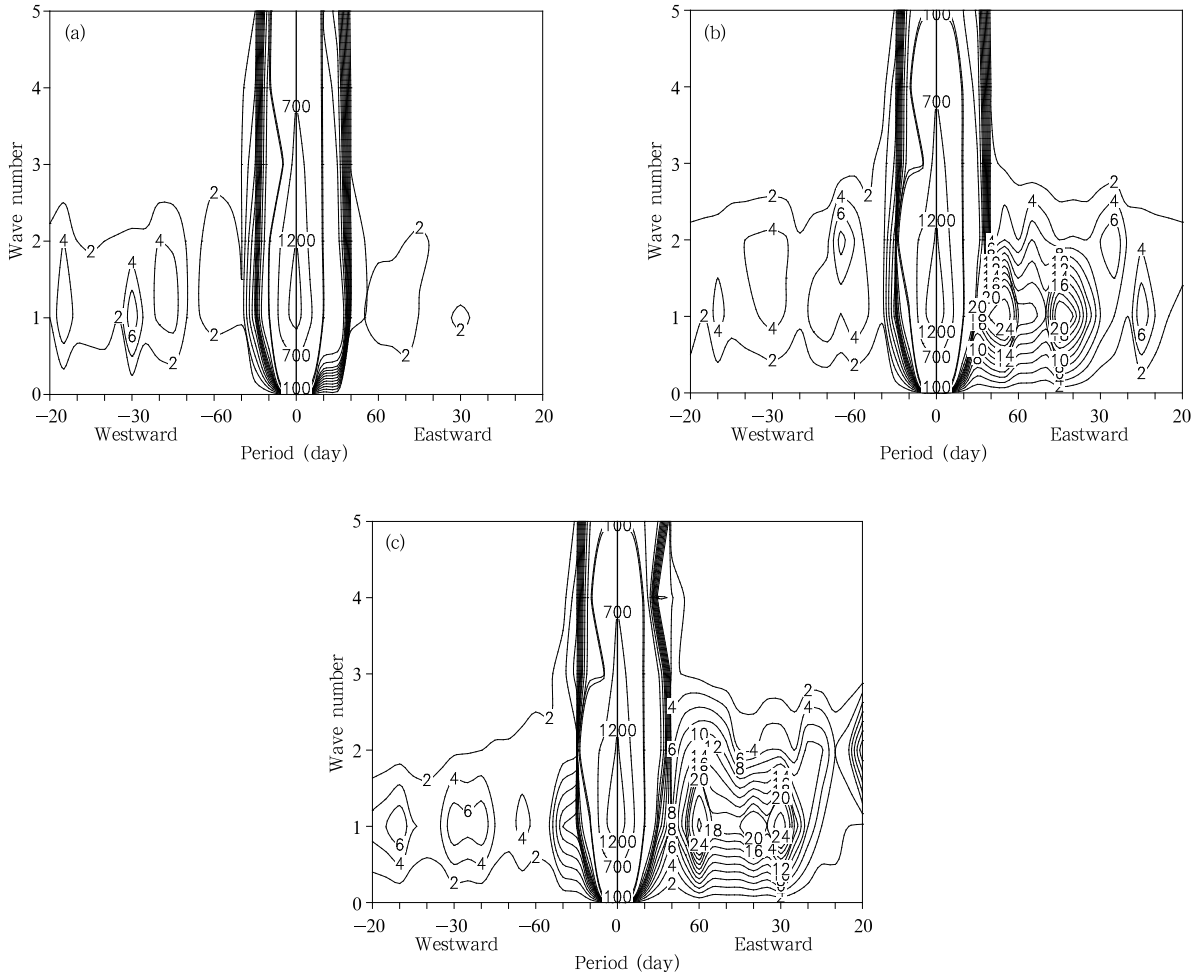

Fig.16. Space-time power spectra of 30–60-day band-pass filtered 850-hPa zonal wind averaged over 10°S–10°N (unit:m^2 s^{-2}) for experiments (a) UH, (b) MH, and (c) LH.

an amplitude much weaker than the observed (Rajendran et al., 2002; Sperber, 2004). Recently, Zhang et al (2005) modified this scheme, and results showed that the modified scheme in CCM3 improved the simulation of MJO.

In the present study, the MCA and ZM (1995) schemes are compared in a single model, and results show that the MCA scheme gives a relatively better simulation of MJO than the ZM scheme. One of the important factors is that the vertical structure of the diabatic heating produced by the two schemes is dramatically different. The MCA scheme produces the maximum heating rate in the middle troposphere, while heating rate produced by the ZM scheme is nearly uniform in the whole troposphere, therefore, no obvious peak level of maximum heating can be seen and the heating rate at every level is too weak, which maybe leads to the weak amplitude of the simulated MJO. Of course, experiments in the present paper mainly investigate impacts of different vertical distributions of heating on the simulated MJO, but do not consider the impacts from different strength of heating. The heating strength in the present paper (about 3–4 K day^{-1}) can be considered as the case of moderate heating, and generally speaking, the stronger the heating is, the stronger the response of atmosphere will be. Anyway, experiments indicate that the simulated MJO by the GCM to some extent is dependent on the vertical structure of the diabatic heating produced by the model, and the heating structure in the model is

mainly determined by the cumulus parameterization scheme.

REFERENCES

Arakawa, A., and W. H. Schubert, 1974: Interaction of a cumulus cloud ensemble with the large-scale environment. Part I. *J. Atmos. Sci.*, **31**, 674–701.

Chao, W. C., and S. J. Lin, 1994: Tropical intraseasonal oscillation, super cloud cluster, and cumulus convection schemes. *J. Atmos. Sci.*, **51**, 1282–1297.

Dong Min, Zhang Xingqiang, and He Jinhai, 2004: A diagnostic study on the temporal and spatial characteristics of the tropical intraseasonal oscillation. *Acta Meteor. Sinica*, **62**(6), 821–830. (in Chinese)

Edwards, J. M., and A. Slingo, 1996: Studies with a flexible new radiation code. I: Choosing a configuration for a large-scale model. *Quart. J. Roy. Meteor. Soc.,* **122**, 689–719.

Guang J. Z., and M. Q. Mu, 2005: Simulation of the Madden-Julian oscillation in the NCAR CCM3 using a revised Zhang-McFarlane convection parameterization scheme. *J. Climate*, **18**, 4046–4064.

Hack, J., 1994: Parameterization of moist convection in the National Center for Atmospheric Research community model (CCM2). *J. Geophys. Res.*, **99**, 15551–15568.

Hendon, H. H., and M. L. Salby, 1994: The life cycle of the Madden-Julian oscillation. *J. Atmos. Sci.*, **51**, 2225–2237.

Holtslag, A. A. M., and B. Boville, 1993: Local versus nonlocal boundary-layer diffusion in a global climate model. *J. Climate*, **6**, 825–1842.

Jia Xiaolong, Li Chongyin, and Zhou Ningfang, 2004: A GCM study on the tropical intraseasonal oscillation. *Acta Meteor. Sinica*, **62**(6), 725–739. (in Chinese)

Jones, C., and B. C. Weare, 1996: The role of low-level moisture convergence and ocean latent heat fluxes in the Madden and Julian oscillation: An observational analysis using ISCCP data and ECMWF analysis. *J. Climate*, **9**, 3086–3104.

Kalnay, E., and Coauthors, 1996: The NCEP/NCAR 40-year reanalysis project. *Bull. Amer. Meteor. Soc.*, **77**, 437–471.

Kuo, Y. H., 1974: Further studies of the parameterization of the influence of cumulus convection on large-scale flow. *J. Atmos. Sci.*, **31**, 1232–1240.

Lau, K. M., and L. Peng, 1987: Origin of low frequency (intraseasonal) oscillation in the tropical atmosphere. Part I: Basic theory. *J. Atmos. Sci.*, **44**, 950–972.

Lee Myong-In, In-Sik Kang, and Brain E. Mapes, 2003: Impacts of cumulus convection parameterization on aqua-planet AGCM simulations of tropical intraseaosnal variability. *J. Meteor. Soc. Japan*, **81**, 963–992.

Li Chongyin, 1983: Convection condensation heating and unstable modes in the atmosphere. *Chinese J. Atmos. Sci.,* **7**, 260–268. (in Chinese)

Li Chongyin, 1991: *Atmospheric Low Frequency Oscillation.* China Meteorological Press, Beijing, 265 pp. (in Chinese)

Li Chongyin, Jia Xiaolong, and Dong Min, 2006: Numerical simulation and comparison study of the atmospheric intraseasonal oscillation. *Acta Meteor. Sinica*, **64**(4), 412–419. (in Chinese)

Li Wei and Yu Yongqiang, 2001: Intraseasonal oscillation in a coupled general circulation model. *Chinese J. Atmos. Sci.*, **25**(1), 118–131. (in Chinese)

Liu Ping, Bin Wang, Kenneth R. Sperber, Tim Li, and Gerald A. Meehl, 2005: MJO in the NCAR CAM2 with the Tiedtke convection scheme. *J. Climate*, **18**, 3007–3020.

Liu Yunyun, Yu Yongqiang, He Jinhai, et al., 2006: Characteristics and numerical simulation of the tropical intraseasonal oscillation under global warning. *Acta Meteor. Sinica*, **64**(6), 412–419. (in Chinese)

Madden, R. A., and P. R. Julian, 1971: Detection of a 40–50-day oscillation in the zonal wind in the tropical Pacific. *J. Atmos. Sci.*, **28**, 702–708.

Madden, R. A., and P. R. Julian, 1972: Description of global scale circulation cells in the tropics with 40-50 day period. *J. Atmos. Sci.*, **29**, 1109–1123.

Madden, R. A., and P. R. Julian, 1994: Observations of the 40-50-day tropical oscillation-A review. *Mon. Wea. Rev.*, **122**, 814–837.

Maloney, E. D., and D. L. Hartmann, 1998: Frictional moisture convergence in a composite life cycle of the Madden-Julian oscillation. *J. Climate*, **11**, 2387–2403.

Maloney, E. D., and D. L. Hartmann. 2001: The sensitive of intraseasonal variability in the NCAR CCM3 to changes in convection parameterization. *J. Climate*, **14**, 2015–2034.

Maloney, E. D., 2002: An intraseasonal oscillation composite life cycle in the NCAR CCM3.6 with modified convection. *J. Climate*, **15**, 964–982.

Manabe, S., J. Smagorinsky, and R. F. Strickler, 1965: Simulated climatology of general circulation model with a hydrologic cycle. *Mon. Wea. Rev.,* **93**, 769–798.

Matthews, A. J, 2000: Propagating mechanisms for the Madden-Julian oscillation. *Q. J. Royal Meteor. Soc.*, **126**, 2637–2651.

Numaguti, A., M. Takahashi, T. Nakajima, and A. Sumi, 1995: Development of an atmospheric general circulation model. In Reports of a New Program for Creative Basic Research Studies, Studies of Global Environment Change with Special Reference to Asia and Pacific Regions, Rep. I-3, Center for Climate System Research, Tokyo, 1–27.

Park, C. K., D. M. Straus, K. M. Lau, et al., 1990: An evolution of the structure of tropical intraseasonal oscillation in three general circulation models. *J. Meteor. Soc. Japan*, **68**, 403–417.

Qu Shujun and Zhang Ming, 2004: The temporal and spatial characteristics of Madden and Julian Oscillation (MJO) in IAP9L AGCM. *Climatic and Environmental Research*, **9**, 567–574. (in Chinese)

Rajendran, K., R. S. Nanjundiah, and J. Srinivasan, 2002: Comparison of seasonal and intraseasonal variation of tropical climate in NCAR CCM2 GCM with two different cumulus schemes. *Meteorology and Atmospheric Physics*, **79**, 57–86.

Rui, H., and B. Wang, 1990: Development characteristics and dynamic structure of tropical intraseasonal convection anomalies. *J. Atmos. Sci.*, **47**, 357–379.

Salby, M. L., and H. H. Hendon, 1994: Intraseasonal behavior of clouds, temperature, and motion in the tropics. *J. Atmos. Sci.*, **51**, 2207–2224.

Slingo, J. M., 1980: A cloud parameterization scheme derived from GATE data for use with a numerical model. *Q. J. Royal Meteor. Soc.*, **106**, 747–770.

Slingo, J. M., 1987: The development and verification of a cloud prediction scheme for the ECMWF model. *Q. J. Royal Meteor. Soc.*, **113**, 899–927.

Slingo, J. M., and Coauthors. 1996: Intraseasonal oscillation in 15 atmospheric general circulation models: Results from an AMIP diagnostic subproject. *Climate Dynamics*, **12**, 325–357.

Sperber, K. R., 2003: Propagation and the vertical structure of the Madden-Julian Oscillation. *Mon. Wea. Rev.*, **131**, 3018–3037.

Sperber, K. R., 2004: Madden-Julian variability in NCAR CAM 2.0 and CCSM2.0. *Climate Dyn.*, **23**, 259–278.

Sud, Y. C., and G. K. Walker, 1999: Microphysics of clouds with the relaxed Arakawa-Schubert Scheme (McRAS). Part I: Design and evaluation with GATE phase III data. *J. Atmos. Sci.*, **56**, 3196–3220.

Sui C. H., and K-M. Lau, 1989: Origin of low frequency (intraseasonal) oscillation in the tropical atmosphere. Part II: Structure and propagation by mobile wave-CISK modes and their modification by lower boundary forcings. *J. Atmos. Sci.*, **46**, 37–56.

Tiedtke, M., 1989: A comprehensive mass flux scheme for cumulus parameterization in large-scale models. *Mon. Wea. Rev.*, **117**, 1779–1800.

Wang, W., and M. E. Schlesinger, 1999: The dependence on convection parameterization of the tropical intraseasonal oscillation simulated in the UIUC 11-layer atmospheric GCM. *J. Climate*, **12**, 1423–1457.

Wang Zaizhi, Wu Guoxiong, Liu Ping, and Wu Tongwen, 2005: The development of Goals/LASG AGCM and its global climatological features in climate simulation I–Influence of horizontal resolution. *Journal of Tropical Meteorology*, **21**(3), 225–237. (in Chinese)

Wu, G. X., H. Liu, Y. C. Zhao, and W. P. Li, 1996: A nine-layer atmospheric general circulation model and its performance. *Adv. Atmos. Sci.*, **13**(1), 1–18.

Wu Guoxiong, Zhang Xuehong, Liu Hui, et al., 1997: Global ocean-atmosphere-land system model of LASG (GOALS/LASG) and its performance in simulation study. *Quarterly Journal of Applied Meteorological* (suppl.), 15–28. (in Chinese)

Xie, P., and P. A. Arkin, 1997: Global precipitation: A 17-year monthly analysis based on gauge observations, satellite estimates, and numerical model output. *Bull. Amer. Meteor. Soc.*, **78**, 2539–2558.

Xue Feng, Liang Xinzhong, Wang Wanqiu, et al., 1996: A numerical simulation of low frequency oscillations in the atmosphere. *Chinese J. Atmos. Sci.*, **20**, 654–661. (in Chinese)

Zhou Tianjun, Yu Rucong, Wang Zaizhi, et al., 2005: *Atmospheric General Circulation Model and Coupled Model FGOALS-s.* China Meteorological Press, Beijing, 288 pp. (in Chinese)

Zhang, G. J., and N. A. McFarlane, 1995: Sensitivity of climate simulation to the parameterization of cumulus convection in the Canadian Climate Centre General Circulation Model. *Atmos-Ocean*, **33**, 407–446.